Improved wavefront estimation accuracy in a programmable grating array based wavefront sensor

OPEN ACCESS
IOP Publishing
Journal of Optics
J. Opt. **23** (2021) 045604 (10pp)
https://doi.org/10.1088/2040-8986/abeec4

Improved wavefront estimation accuracy in a programmable grating array based wavefront sensor

Biswajit Pathak*

Department of Engineering Science, University of Oxford, Parks Road, Oxford OX1 3PJ, United Kingdom

E-mail: biswajit.pathak@eng.ox.ac.uk

Received 29 December 2020, revised 21 February 2021
Accepted for publication 15 March 2021
Published 30 March 2021

Abstract

Shack–Hartmann wavefront sensor (SHWS) is one of the popular zonal wavefront sensor that typically consists of a two-dimensional (2D) array of lenslets and a camera. Another variant of a zonal wavefront sensor is the programmable grating array based wavefront sensor (PGAWS) that replaces the lenslets array of the SHWS with a 2D array of programmable diffraction gratings and a single focusing lens to result in a 2D array of $+1$ order spots. The ability of a PGAWS to correctly measure the incident wavefront depends on the accuracy with which each $+1$ order spot centroid position in the camera plane is calculated. However, in practical applications the intensities of the $+1$ order spots are usually non-uniform and there is presence of higher order spots that lead to erroneous calculation of the centroid position. In the present work, an improved PGAWS is proposed and by exploiting its programmable facility the transmittance function of the grating array is defined to generate an array of uniform intensity $+1$ order spots with negligible contribution from unwanted higher order spots by breaking them into noise. We present proof-of-concept simulation results that illustrate the generation of uniform intensity $+1$ order spots and also quantify its uniformity numerically by defining a quality metric. Furthermore, the working of the proposed PGAWS is substantiated through simulation results which demonstrate its accurate wavefront estimation capability in comparison to the conventional PGAWS, in the presence of non-uniform intensity $+1$ order spots.

Keywords: Shack–Hartmann wavefront sensor, diffraction grating, centroid, wavefront estimation

(Some figures may appear in colour only in the online journal)

1. Introduction

The Shack–Hartmann wavefront sensor (SHWS) is a widely used zonal wavefront sensor [1] which finds application in different areas such as ophthalmology [2, 3], astronomy [4], optical miscroscopy [5, 6], laser beam characterisation [7], optical trapping [8], etc. It basically consists of a two-dimensional (2D) array of lenslets together with a camera which is placed at the common focal plane of the lenslets. In an ideal situation, when an unaberrated wavefront (also referred to as plane wavefront) illuminates the lenslets array, a uniform pattern of spots is generated on the focal plane of the lenslets array (reference spots). However, if there is any deviation in the incident wavefront (distorted with respect to the plane wavefront) then the focal spots will be displaced from

* Author to whom any correspondence should be addressed.

their original positions, proportional to the tilt of the wavefront across its lenslets aperture (shifted spots). The amount of displacement between the shifted and reference focal spot centroid positions will provide important information about the local wavefront slopes of the incident wavefront. This slope information can be effectively used in a zonal or modal wavefront estimation algorithm [9–11] to generate the phase profile of the incident wavefront.

A zonal wavefront sensor can also be implemented by using a liquid crystal spatial light modulator (LCSLM) which can be used to realize an array of binary diffractive lenses [12–14]. It is shown that an array of 2D plane diffraction gratings (implemented with an LCSLM) together with a single focusing lens instead of the lenslet array in the SHWS can be used to design a programmable grating array based wavefront sensor (PGAWS) [15, 16]. If a collimated laser beam is incident on the grating array, it generates a number of diffracted orders such as ±1, ±3, ±5, etc. Among the various diffracted orders, the $+1$ order from each grating element is primarily chosen (due to its high intensity) to result in a regular 2D array of focal spots in the camera plane for an unaberrated incident wavefront. The PGAWS works in a similar principle as that of the SHWS with some added advantages such as flexibility in the camera geometry [17, 18], ability to enhance the spatial resolution [19] and accuracy [20], owing to its programmable nature. However, there are also some limitations associated with the conventional design of PGAWS that results in fixed intensity of the $+1$ order spots and presence of undesirable higher order spots which adversely affects the centroid calculation.

The accurate centroid calculation is very important in deciding the correctness of the wavefront measured by a zonal wavefront sensor, as the accuracy with which the wavefront slope is calculated is dependent on the accurate calculation of the focal spot centroid position [21, 22]. Else, the error due to inaccurate centroid calculation will propagate through the wavefront estimation algorithm to result in an inaccurate estimation of the wavefront [11, 23]. It is noteworthy that the centroid calculation will become erroneous if the intensity of the focal spots in a zonal wavefront sensor is not optimum, i.e. there is presence of either faint or saturated spots [24, 25]. Thus, the signal-to-noise ratio (SNR) of these focal spots will not be uniform to calculate each centroid position with enough accuracy. During the calculation of centroid position, the focal spots with low SNR are generally not taken into account which leads to significant loss of information [26]. This process eventually results in an additional error as the information from these spots is generally extrapolated in the wavefront estimation process. A solution to obtain an array of focal spots with equivalent SNR, is by capturing a sequence of focal spot images with different exposure times of the camera [25]. However, such an approach need multiple camera frames and makes the process more complex. There are a number of practical situations where the intensity of the focal spots (or the $+1$ orders spots) in a zonal wavefront sensor may not be uniform [27] such as in ophthalmic wavefront sensing [28, 29], transmitted light in an optical fiber [27], unevenly coated optical elements [30], thin film measurement system [31]. It is to be mentioned that the centroid calculation for non-uniform $+1$ order spot intensities in a PGAWS will be more affected than the centroid calculation for non-uniform focal spot intensities in a SHWS. This is because there is presence of unwanted higher order spots in PGAWS. The intensity value of these higher order spots will either get incorporated into the centroid calculation along with the $+1$ order spots, or their contribution will be removed along with the necessary $+1$ order spots, when applying a threshold value to remove the higher order spots.

In the present work, we propose a grating array based wavefront sensor to obtain uniform intensity $+1$ order spots with negligible contribution from undesired higher order spots. Using the proposed sensor, we can independently manipulate the intensity of each $+1$ order spot by varying the duty cycle of its corresponding diffraction grating element. Moreover, random binarisation of the diffraction grating array is implemented to reduce the contribution from undesired higher order spots by breaking them into noise. Working of the proposed sensor is illustrated through simulation results that show generation of uniform intensity $+1$ order spots. Furthermore, a quality metric is defined to quantify the uniformity in $+1$ order intensities numerically. We also present simulation results that demonstrate accurate wavefront estimation capability of the proposed PGAWS in comparison to the conventional PGAWS, in the presence of non-uniform intensity $+1$ order spots.

2. Methodology

In this section, we first present the design of a PGAWS and this will be followed by the manipulation of $+1$ order intensities to obtain an array of uniform intensity $+1$ order spots. Next, random binarisation of the grating array is presented to reduce the contribution of diffraction effects from higher order spots.

2.1. Design of grating array based wavefront sensor

By using the principle of computer generated holography (CGH) technique, a user defined wavefront can be generated [32, 33]. Let, us represent the complex amplitude of the object beam, with unit amplitude as

$$A(x,y) = e^{[i\{\phi(x,y)+\tau(x,y)\}]}. \tag{1}$$

Here, $\phi(x,y)$ represents the user defined phase function and $\tau(x,y)$ represents the linear tilt function, in the hologram plane. The user defined phase function represents the classical aberrations expressed as a linear combination of an orthogonal basis function, such as Zernike polynomials [34]. If we do not consider the user defined phase function, i.e. $\phi(x,y) = 0$, then the hologram simply represents a plane binary diffraction grating pattern. This corresponds to an unaberrated wavefront deflected to a particular direction determined by the tilt function. The tilt function, $\tau(x,y) = f_{0x}x + f_{0y}y$, represents the amount of deflection of the desired order with respect to the undiffracted zero order. The amount of deflection of the desired order along the horizontal direction and vertical direction is described by the values of the spatial

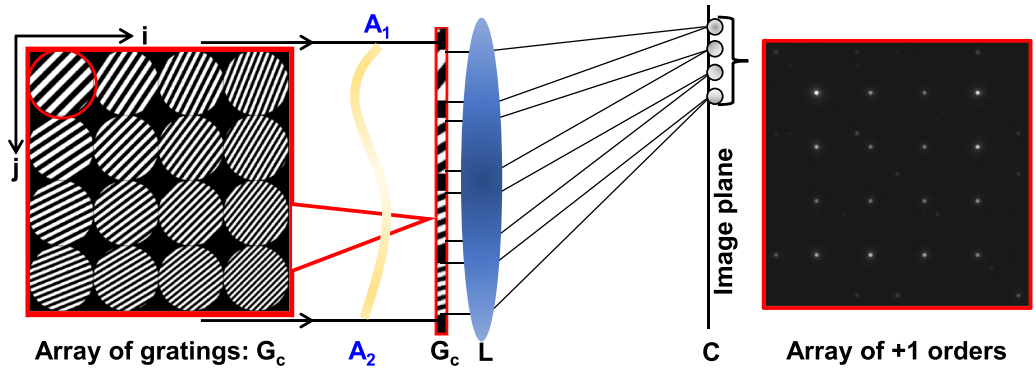

Figure 1. Schematic diagram of the conventional PGAWS. The transmittance profile of the grating array having 4×4 number of gratings and the corresponding $+1$ order spots of dimension 4×4 are shown on the extreme left and right of the figure respectively.

frequencies, f_{0x} and f_{0y}, respectively. This facilitates in the construction of a 2D array of binary diffraction gratings in which the spatial frequencies of each grating element can be configured to result in a 2D array of nth diffracted orders. Thus, the mathematical algorithm defining the transmittance function of the 2D array of diffraction grating pattern $g_t(x, y)$, binarised to generate an array of n diffracted orders can be written as

$$g_t(x,y)\Big|_{(i,j)=(1,1)}^{(i,j)=(N,N)} = \begin{cases} 1 & \text{if} \cos\left[\phi^{i,j}(x,y) + (f_{0x}^{i}x + f_{0y}^{j}y)\right] \geqslant 0 \\ 0 & \text{if} \cos\left[\phi^{i,j}(x,y) + (f_{0x}^{i}x + f_{0y}^{j}y)\right] < 0 \end{cases} \tag{2}$$

where (N, N) denotes the grating array dimension, $\phi^{i,j}(x, y)$ represents the phase of each grating element (here $\phi^{i,j}(x, y) = 0$) and (f_{0x}^{i}, f_{0y}^{j}) is given as

$$\begin{aligned} f_{0x}^{i} &= f_{0x}^{1} + (i-1) \times \Delta f_{0x} \\ f_{0y}^{j} &= f_{0y}^{1} + (j-1) \times \Delta f_{0y}. \end{aligned} \tag{3}$$

Here, (f_{0x}^{1}, f_{0y}^{1}) is the spatial frequency of the top left grating element (i.e. 1,1) and $(\Delta f_{0x}, \Delta f_{0y})$ are real numbers that apply a uniform increment between the adjacent grating elements along i (row index) and along j (column index). When focused by a lens, it will result in various odd diffracted orders in the image plane. For $\Delta f_{0x} = \Delta f_{0y}$, the resulting $\pm n$ diffracted orders ($n = \pm 1, \pm 3, \pm 5, \ldots$) will form a square array of dimension $N \times N$ for an unaberrated incident beam. The formation of the diffracted orders in the image plane can be explained by performing a Fourier series expansion of the transmittance function of the grating [17, 33]. Each of these orders are diffracted to spatially separated positions as each diffracted order contains a different overall tilt. Thus, the diffraction orders $\pm n$ are located at relative distances of $\pm n$ with respect to the undiffracted zero order. The diffracted orders have relative intensities $(\frac{1}{n\pi})^2$ and carry relative phases $\pm n\phi$. Thus, each of the increasing diffracted order carries a phase information ϕ that is scaled with the same order. The location of any of the $\pm n$ diffracted order with respect to the undiffracted zero order is a function of the spatial frequencies, f_{0x} and f_{0y} and the order of diffraction. Thus, if an array of grating elements are arranged in a regular 2D structure, similar to the lenslets array structure in the case of SHWS and if the spatial frequency of each of the grating elements are properly configured, the focal spots corresponding to the nth diffraction order can be made to form a regular 2D array (in the case of an unaberrated incident wavefront). We assume that the size of each grating element is small enough in comparison to the curvature of the incident wavefront sampled across its grating aperture. In such a case, the portion of the incident wavefront across each grating element will offer a slope relative to the plane of the grating element. This will result in the shift of the location of $\pm n$ diffracted order in proportion to the amount of slope received by each grating element (due to wavefront deformation or holographically added phase profile). Here, $+1$ order spots have been considered but, diffracted spots of any order may serve the purpose of forming the 2D array of focal spots. Therefore, the 2D array of $+1$ order spots generated can be considered to be similar to the focal spot array in the case of SHWS. Thus, we replace the tiny array of lenslets of the SHWS by an array of small binary diffraction grating patterns, together with a single focusing lens. Moreover, the transmittance functions for the same $N \times N$ grating array can be configured to form lesser number of focal spot rows than that in a conventional SHWS [17, 18].

A diagrammatic representation of the principle of wavefront sensing using 2D array of binary diffraction grating pattern has been illustrated in figure 1. A collimated light beam incident on the 2D binary grating array G_c gets diffracted and is finally focused by lens L onto the image plane where a camera C is placed. The spatial frequencies are configured according to equation (2) to form a regular 2D array of focal spots in the case of unaberrated incident wavefront. If we consider an incident wavefront with non-uniform intensity distribution profile, represented by A_1A_2 across the grating aperture, then the resulting $+1$ order spots will also have non-uniform intensities in the image plane. It is noteworthy that apart from the $+1$ order spots, there will be presence of higher order spots which are generally eliminated by putting a threshold. Therefore, in the presence of a wavefront with non-uniform intensity distribution, putting an improper threshold value will avoid contribution from necessary $+1$ order spots, whereas without the threshold the contribution from higher order spots will get incorporated into the centroid calculation.

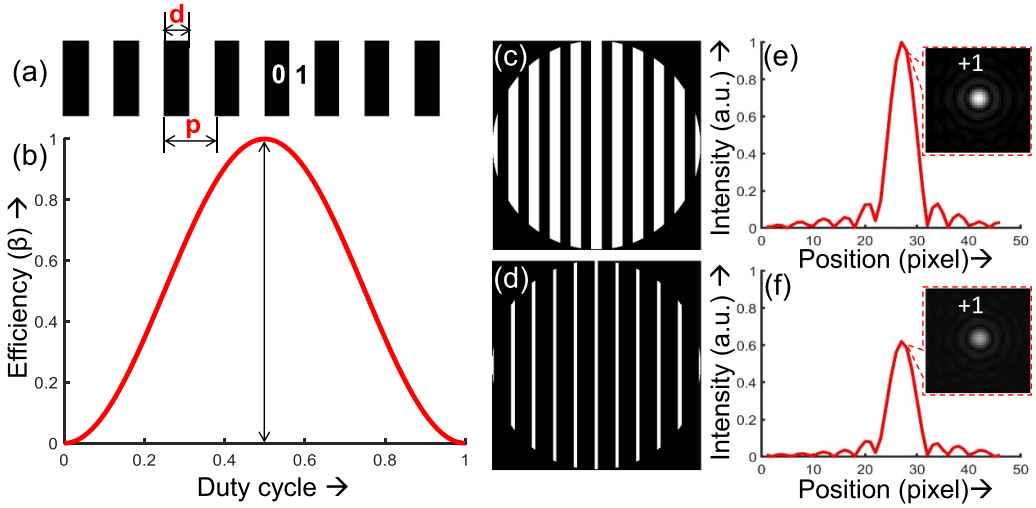

Figure 2. A representative binary diffraction grating pattern with a (a) controllable duty cycle and the (b) diffraction efficiency plot of its corresponding $+1$ order spot as a function of duty cycle. The binary diffraction grating element with (c) $D_c = 0.5$ and (d) $D_c = 0.7$ and the corresponding line plots across the center of $+1$ order spot for (e) $D_c = 0.5$ and (f) $D_c = 0.7$ are shown, respectively.

This will adversely affect the wavefront estimation process as the centroid position information is an important parameter for wavefront slope measurement. Thus, the PGAWS as shown in figure 1, constructed using the transmittance function given by equation (2) consists of an array of gratings (G_c) that results in an array of $+1$ order spots with fixed intensity (due to fixed duty cycle) and with no provision to reduce the effect of higher order spots. We refer to such a sensor as a conventional PGAWS.

2.2. Grating array with controllable $+1$ order spot intensities

In order to address the issue of fixed intensity as mentioned above, we demonstrate how the intensity of the $+1$ order spot can be manipulated by changing the width of the transmittance portion of the diffraction grating, which is also known as the duty cycle. The duty cycle of a binary diffraction pattern is defined as the ratio of the opaque or transmittance width to the period of the grating pattern, i.e. $D_c = \frac{d}{p}$ as shown in figure 2(a). The black portion represents a transmittance value of 0 whereas the white portion represents a transmittance value of 1. The efficiency of the $+1$ order spot as a function of the duty cycle and the order number [35] is given by equation (4). The variation of β as a function of D_c for $n = 1$ (i.e. $+1$ order spot) is plotted in figure 2(b). From the plot, it is evident that the diffraction efficiency reaches a maximum value for $D_c = 0.5$ and minimum values for $D_c = 0$ and $D_c = 1$. Figures 2(c) and (d) represents the binary diffraction grating element with $D_c = 0.5$ and $D_c = 0.7$ and the respective line plots corresponding to the center of $+1$ order spot are shown in figures 2(e) and (f), respectively.

$$\beta = \left(\frac{d}{p}\right)^2 \times \mathrm{sinc}^2\left(\frac{nd}{p}\right). \tag{4}$$

We redefine the transmittance function of the array of binary diffraction gratings with variable duty cycle (while retaining the meaning of the variables as mentioned earlier), as given below

$$g_t(x,y)\Big|_{(i,j)=(1,1)}^{(i,j)=(N,N)} = \begin{cases} 1 & \text{if} \cos\left[\phi^{i,j}(x,y) + (f_{0x}^i x + f_{0y}^i y)\right] \geqslant \sqrt{1 - I_{i,j}^2} \\ 0 & \text{if} \cos\left[\phi^{i,j}(x,y) + (f_{0x}^i x + f_{0y}^i y)\right] < \sqrt{1 - I_{i,j}^2} \end{cases} \tag{5}$$

where $I_{i,j}$ represents the desired intensity of the $+1$ order spot corresponding to the (i,j)th grating element such that a minimum and maximum intensity of the $+1$ order spot can be either 0 or 1, respectively. Using equation (5) we can vary the duty cycle of any of the grating element to obtain a desired intensity of the $+1$ order spot [35, 36]. Thus, we can independently control the intensity of each $+1$ order spot so that the intensity of the entire array of $+1$ orders can be uniformised. Therefore, irrespective of the incident beam intensity profile we can obtain uniform intensity $+1$ order spots.

2.3. Random binarisation of the diffraction grating array

In order to address the issue of presence of higher order spots in the case of conventional PGAWS, we implement random binarisation to the transmittance function of the grating array given by equation (5), such that the higher order spots can be reduced to noise by breaking down the periodicity of the diffraction grating pattern [37–40]. The presence of higher order spots is basically a result of using highly structured diffraction grating pattern. Thus, introduction of random numbers into the binarisation of the grating array reduces the presence of undesired higher order spots. This can be achieved by following the mathematical relation as given by equation (6) below,

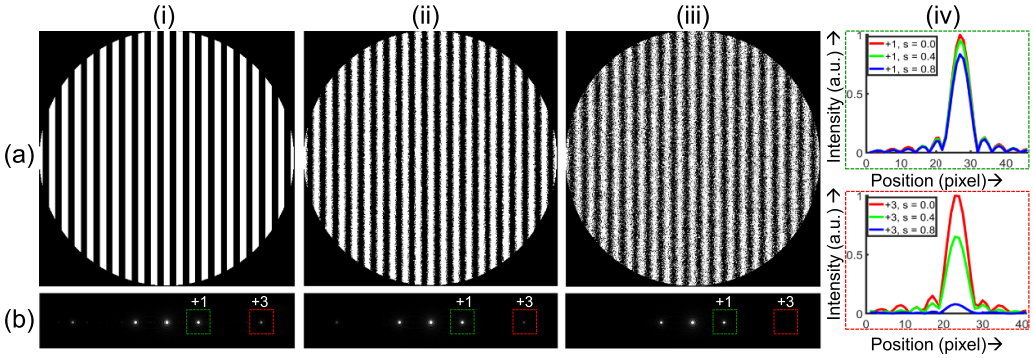

Figure 3. An illustration showing the reduction of intensity of the higher order spots before and after implementation of random binarisation. The binary diffracting grating element with (i)(a) $s = 0$, (ii)(a) $s = 0.4$ and (iii)(a) $s = 0.8$ and the corresponding diffracted spots are shown in (i)(b), (ii)(b) and (iii)(b), respectively. The normalised intensity plots of the $+1$ order spot and the $+3$ order spot (shown in (b)) for different values of s are shown in (iv)(a) and (iv)(b), respectively.

$$H_R(i,j) = \begin{cases} 1 & \text{if} g_t^{i,j}(x,y) \geqslant sR_n(x,y) \\ 0 & \text{if} g_t^{i,j}(x,y) < sR_n(x,y) \end{cases} \tag{6}$$

where R_n represents a uniform distribution of random numbers between 0 and 1, and s is a real number with values ranging between 0 and 1 which can be used to scale the amplitude of random binarisation so that the effect from higher order spots become negligible. We illustrate the effect of randomisation on higher order spots considering a single grating element as shown in figure 3. Figures 3(i)(a)–(iii)(a) represents the binary diffracting grating element with $s = 0$, $s = 0.4$ and $s = 0.8$, respectively and the corresponding diffracted spots are shown in figures 3(i)(b)–(iii)(b), respectively. Figures 3(iv)(a) and (iv)(b) shows the normalised intensity plots of the $+1$ order spot and the $+3$ order spot (shown in (b)) for different values of s, respectively. From, figure 3(i)(b) it is evident that the intensity of higher order spot (i.e. $+3$) is significant for $s = 0$, prior to implementation of random binarisation. However, as we go on increasing the value of s, the intensity decreases gradually as evident from figures 3(ii)(b) and (iii)(b). The decrease in relative intensity of the $+3$ order spot with the increase in the value of s can be clearly observed from the line plots shown in figure 3(iv)(b). It is to be noted that, random binarisation of the diffraction grating array introduces random background noise whose magnitude is very small and this can be eliminated by putting a threshold. Moreover, the random binarisation also reduces the intensity of the $+1$ order spots as shown in figure 3(iv)(a) which is again relatively small (i.e. $\frac{1}{n^2\pi^2}$) when compared to the decrease observed in the case of higher order spots ($n = \pm 3, \pm 5$, etc), so it does not pose a significant issue. Hence, by using equations (5) and (6) consecutively, we can manipulate the intensity of desired $+1$ order spot of the array and reduce the effect of diffraction from higher order spots.

Figure 4 represents a schematic diagram of the proposed PGAWS, where the conventional 2D grating array is replaced with the modified 2D grating array, G_p generated by using equations (5) and (6) consecutively. Thus, such an arrangement generates uniform intensity $+1$ order spots with negligible contribution from higher order spots.

3. Results and discussion

We perform simulations to illustrate the working of the conventional and the proposed PGAWS. For this purpose, we have considered three illumination intensity distribution profiles, namely, super-Gaussian, Gaussian and non-Gaussian to generate $+1$ order spots with uniform (super-Gaussian) and non-uniform (Gaussian and non-Gaussian) intensities. Numerical simulations were performed in MATLAB by taking Fourier Transform operations over the binary diffraction grating array having dimensions of 6×6 defined with a total pixel resolution of 1024×1024 (equivalent to a typical LCSLM pixel resolution) to generate the array of $+1$ order spots. Prior to implementation of the proposed PGAWS, we record the array of $+1$ order spots with a constant duty cycle. This may result in both saturated and faint $+1$ order spots corresponding to a non-uniform intensity profile of the incident beam. Then the intensity of the $+1$ order spots are scaled by a constant factor so that the spot with minimum intensity (faint spots) is now visible, without saturating them (this process can be performed in an actual experimental setup, either by increasing the laser power or by increasing the exposure time of the camera). This minimum intensity spot should now have a higher signal-to-background noise to perform the centroid calculation and the duty cycle corresponding to this spot is kept unchanged. This process of scaling will also consequently scale the intensity of the brighter $+1$ order spots (already visible earlier) to make them saturated. We then vary the duty cycle of the diffraction grating (G_p) following the relationship between β and D_c in such a way that the intensity of all the spots in the array becomes equivalent to the spot with minimum intensity in that array. We then implement random binarisation to the binary diffraction grating pattern according to equation (6) (based on the maximum intensity of the higher order spots), such that the effect of higher order spots can be eliminated so that they do not contribute toward the centroid calculation process.

Figure 5(i)(a) represents the array of uniform intensity $+1$ order spots obtained using the conventional PGAWS, corresponding to a super-Gaussian illumination intensity profile, so as to have a uniform intensity across the grating

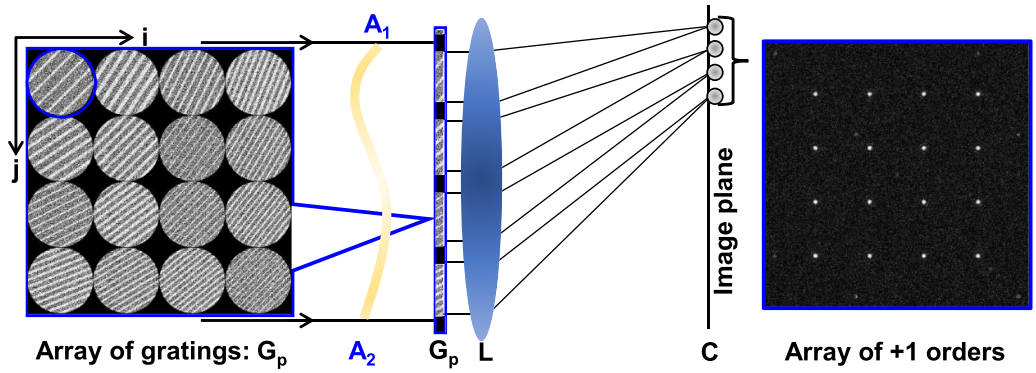

Figure 4. Schematic diagram of the proposed PGAWS. The modified transmittance profile of the grating array having 4×4 number of gratings and the corresponding $+1$ order spots of dimension 4×4 are shown on the extreme left and right of the figure respectively.

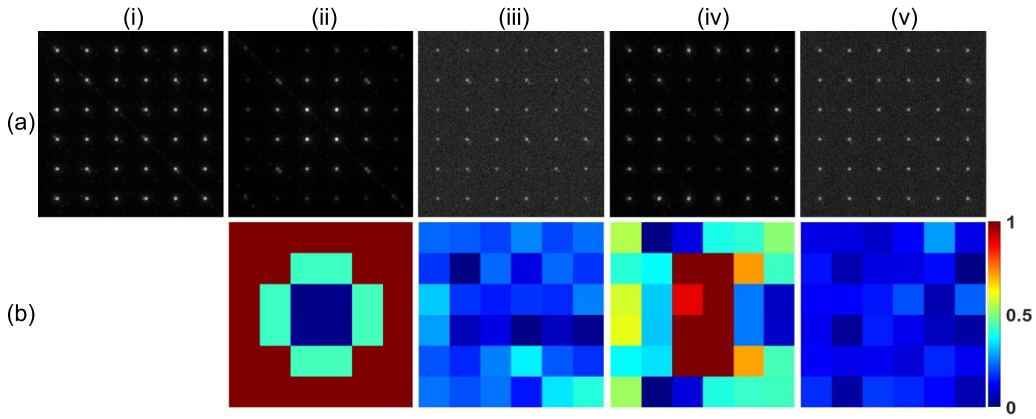

Figure 5. The 2D array of $+1$ order spots obtained using conventional PGAWS with (i)(a) uniform intensity corresponding to a super-Gaussian illumination intensity profile. The 2D array of $+1$ order spots with (ii)(a) non-uniform and (iii)(a) uniform intensities obtained using the conventional PGAWS and proposed PGAWS, respectively, corresponding to a Gaussian illumination intensity profile. Similarly, the 2D array of $+1$ order spots with (iv)(a) non-uniform and (v)(a) uniform intensities obtained using the conventional PGAWS and proposed PGAWS, respectively, corresponding to non-Gaussian illumination intensity profiles. The Q_m evaluated for (ii)(a) to (v)(a) with respect to (i)(a) is shown in (ii)(b) to (v)(b), respectively. The values of the Q_m is normalised and a common colorbar for all the plots in row (b) is shown alongside.

array dimension of 6×6. Similarly, figures 5(ii)(a) and (iv)(a) represents the array of non-uniform intensity $+1$ order spots using the conventional PGAWS, corresponding to Gaussian and non-Gaussian illumination intensity profiles with a beam diameter equivalent to that of the grating array dimension. Figures 5(iii)(a) and (v)(a) represents the array of $+1$ order spots whose intensity has been uniformised and higher order spots have been minimised using the proposed PGAWS, corresponding to the illumination profiles considered in figures 5(ii)(a) and (iv)(a), respectively.

Moreover, to quantify the uniformity in the intensity of $+1$ order spots obtained using the proposed PGAWS in comparison to the conventional PGAWS, we define a quality metric, Q_m, given by the relation,

$$Q_m(p,q) = \left\{ \frac{\sum_{(i=1,j=1)}^{(i=N_i,j=N_j)} I^A(i,j) - \sum_{(i=1,j=1)}^{(i=N_i,j=N_j)} I^B(i,j)}{\sum_{(i=1,j=1)}^{(i=N_i,j=N_j)} I^A(i,j) + \sum_{(i=1,j=1)}^{(i=N_i,j=N_j)} I^B(i,j)} \right\} \quad (7)$$

where, $\sum_{(i=1,j=1)}^{(i=N_i,j=N_j)} I^{A,B}(i,j)$ represents the average of the sum of intensity values within a region that has the same width as the full width at half maximum (FWHM) of a spot with maximum intensity corresponding to figure 5(i)(a), (p,q) denotes the grating subaperture index, (i,j) represents the pixel index, (N_i, N_j) represents the total numbers of pixels in each column and row of the FWHM subaperture, A represents the intensity measured corresponding to super-Gaussian illumination intensity profile and B represents the intensity measured corresponding to Gaussian and non-Gaussian illumination intensity profiles before and after uniformisation.

Initially, the Q_m is evaluated for the array of $+1$ orders spots shown in figures 5(i)(a) and (ii)(a) (now A represents super-Gaussian and B represents Gaussian, before uniformisation) and is shown in figure 5(ii)(b). Next, the Q_m is evaluated between figures 5(i)(a) and (iii)(a) (now A represents super-Gaussian and B represents Gaussian, after uniformisation) and is shown in figure 5(iii)(b). Similarly, the Q_m for non-Gaussian illumination intensity profile before (between

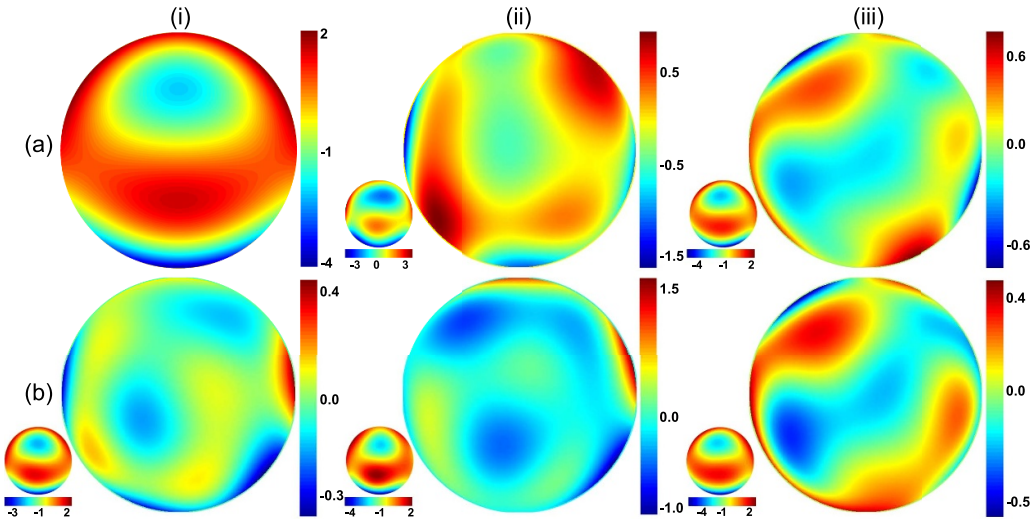

Figure 6. False color images representing the (i)(a) applied phase profile corresponding to Zernike modes $\phi(x,y) = 0.5Z_5 - 1Z_8$ and the (i)(b) 2D error plot obtained using the conventional PGAWS corresponding to super-Gaussian illumination intensity profile. The 2D error plots obtained using the conventional PGAWS in the case of (ii)(a) Gaussian and (ii)(b) non-Gaussian intensity profiles, whereas the 2D error plots obtained using the proposed PGAWS in the case of (iii)(a) Gaussian and (iii)(b) non-Gaussian illumination intensity profiles, have been shown respectively. The estimated phase profiles obtained in each of the cases are shown at the bottom-left of the respective 2D error plots. The axis labels appearing in all the images have the unit of radian.

figures 5(i)(a) and (iv)(a)) and after uniformisation (between figures 5(i)(a) and (v)(a)) is evaluated in the same manner and is shown in figures 5(iv)(b) and (v)(b), respectively. It is evident from the simulation results shown in figure 5(a) that the proposed PGAWS is capable of uniformising the intensity of $+1$ order spots as well as eliminating the contribution from higher order diffracted spots to a significant extent. The same is being quantified and illustrated in figure 5(b) using the quality metric. It is evident from figures 5(iii)(b) and (v)(b) that the values of the Q_m are equivalent when the proposed PGAWS is used, unlike figures 5(ii)(b) and (iv)(b) when the conventional PGAWS is used. Also, it is observed that in figures 5(iii)(a) and (v)(a), there is presence of uniformly distributed small random noise arising from the breakdown of the higher order spots which can now be easily eliminated by putting a threshold value.

We present another set of simulation results that show the wavefront estimation accuracy using the proposed PGAWS in comparison to the conventional PGAWS. The CGH scheme implemented facilitates realising a single $+1$ order beam in the case of a single hologram or an array of $+1$ order beams in the case of an array of holograms where the phase profile of the $+1$ order beam is user defined. Thus, it is possible to generate $+1$ order beams with phase profiles corresponding to user defined monochromatic aberrations. If the grating subapertures are assumed to constitute the resultant aperture of the incident beam over which the aberration function is described, it is possible to generate $+1$ orders corresponding to an unaberrated incident beam which can be assumed to be holographically aberrated with same aberration function. We then use the phase function $\phi(x,y)$ to represent a beam with classical aberrations expressed as a linear combination of single index Zernike polynomials [34], such that $\phi(x,y) = \Sigma a_j Z_j(x,y)$ (where a_j represents the root mean square amplitudes of the jth mode in radians). Initially, we measure the centroid position using the standard center of mass algorithm [22] within the FWHM subaperture (defined corresponding to the maximum intensity of the array) of each $+1$ orders without applying the phase profile (reference spots) and later with the applied phase $\phi(x,y)$ added holographically (shifted spots). The shift of the focal spots are obtained from the two images and the horizontal and vertical slopes are calculated from the focal spot shifts along the horizontal and vertical directions, respectively. From these measured slope information, the applied phase profile is estimated using modal wavefront estimation algorithm [9].

Figure 6 shows the 2D applied phase for $\phi(x,y) = 0.5Z_5 - 1Z_8$ and the 2D error plots obtained by taking the difference between the applied phase and the estimated phase, using the conventional and proposed PGAWS for different illumination intensity profiles. Wavefront estimation is performed using modal wavefront estimation method for grating array dimensions of 6×6. The 2D plot of the applied phase profile $\phi(x,y)$ and the corresponding 2D error plot obtained using the conventional PGAWS in the case of super-Gaussian illumination intensity profile are shown in rows (a) and (b) of column (i). The 2D error plots obtained using the conventional and proposed PGAWS in the case of Gaussian illumination intensity profiles are shown in row (a) of column (ii) and (iii), respectively. Similarly, the 2D error plots obtained using the conventional and proposed PGAWS in the case of non-Gaussian illumination intensity profiles are shown in row (b) of column (ii) and (iii), respectively. The 2D estimated phase profiles for both the conventional and proposed PGAWS for different illumination intensity profiles are shown at the bottom-left of each of the respective 2D error plots. All the plots in figure 6

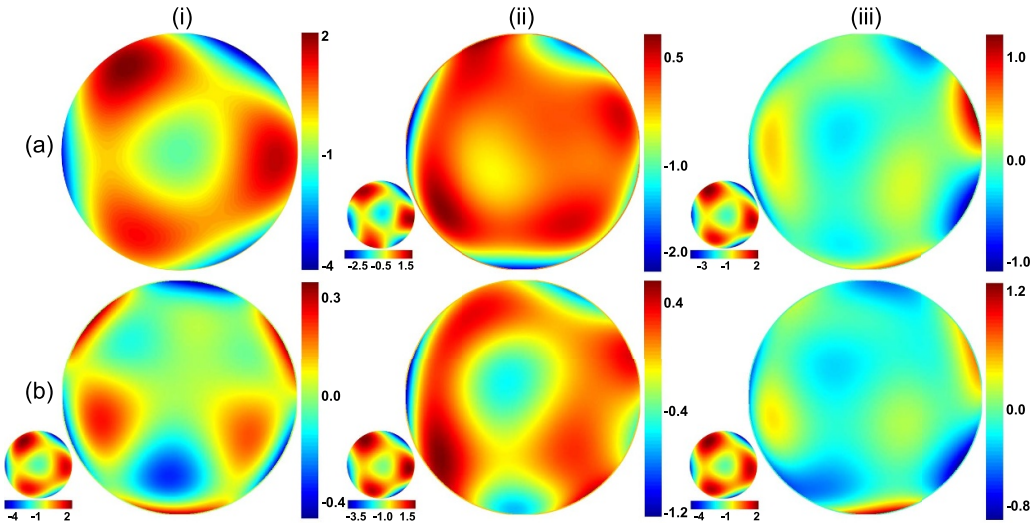

Figure 7. False color images representing the (i)(a) applied phase profile corresponding to Zernike modes $\phi(x,y) = 0.3Z_6 + 0.8Z_9 - 0.6Z_{11}$ and its (i)(b) 2D error plot obtained using the conventional PGAWS corresponding to super-Gaussian illumination intensity profile. The 2D error plots obtained using the conventional PGAWS in the case of (ii)(a) Gaussian and (ii)(b) non-Gaussian intensity profiles, whereas the 2D error plots obtained using the proposed PGAWS in the case of (iii)(a) Gaussian and (iii)(b) non-Gaussian illumination intensity profiles, have been shown respectively. The estimated phase profiles obtained in each of the cases are shown at the bottom-left of the respective 2D error plots. The axis labels appearing in all the images have the unit of radian.

are in radian units. The RMS value of the difference between the applied phase profile and the estimated phase profile is then used to estimate the errors in the measured phase profiles. The value of the RMS error in the case of conventional PGAWS for super-Gaussian illumination intensity profile is 0.0837 radian. Similarly, the value of RMS errors in the case of conventional PGAWS for Gaussian and non-Gaussian illumination intensity profiles are found to be 0.3205 radian and 0.2459 radian, whereas the same in the proposed PGAWS are found to be 0.1867 radian and 0.1662 radian, respectively. A similar result is shown in figure 7 for the applied phase, $\phi(x,y) = 0.3Z_6 + 0.8Z_9 - 0.6Z_{11}$. The value of the RMS error in the case of conventional PGAWS for super-Gaussian illumination intensity profile is 0.1071 radian and the RMS errors in the case of conventional PGAWS for Gaussian and non-Gaussian illumination intensity profiles are found to be 0.3622 radian and 0.2408 radian, whereas the same in the proposed PGAWS are found to be 0.2036 radian and 0.1902 radian, respectively.

Thus, it is observed that the RMS error in the case of proposed PGAWS is smaller in comparison to the conventional PGAWS for both the applied phase profiles in the presence of both Gaussian and non-Gaussian illumination intensity profiles. This is due to the fact that the centroid calculation error in the case of proposed PGAWS is smaller in comparison to the conventional PGAWS. Accurate centroid calculation in the case of proposed PGAWS is possible as the contribution from higher order spots has been significantly minimised and the signal-to-background noise of $+1$ order spots has also been significantly improved. It is to be mentioned that the conventional PGAWS performs better for uniform intensity $+1$ order spots, corresponding to super-Gaussian illumination and when the centroid calculation is performed within the FWHM aperture. However, in a situation where the intensity of the $+1$ order spots is non-uniform, then the proposed PGAWS performs significantly better than the conventional PGAWS. The proposed PGAWS can be implemented experimentally in a similar way as the conventional PGAWS reported earlier [15, 16] by using an LCSLM with sufficient pixel resolution and optimum pixel pitch without compromising on the accuracy and dynamic range of the sensor. It is important to vary D_c based on the pixel pitch so that the grating element with highest spatial frequency can be defined with sufficient pixels and the value of s can be set as per requirement to reduce the contribution from higher order spots. The proposed PGAWS can also be implemented by exploiting the 24 bit-planes (color image) display of a ferroelectric LCSLM [19] and made to work at a frame rate equivalent to that of the standard refresh rate of a video signal. The first bit-plane of the ferroelectric LCSLM can be used to display the binary diffraction grating array corresponding to the conventional PGAWS to record the non-uniform intensity of the $+1$ order spots. The second or any other bit-plane (following a proper firmware deciding the duration and order of display of various bit-planes) can be subsequently used to make the necessary manipulations to result in an array of uniform intensity $+1$ order spots, corresponding to the binary diffraction grating array of the proposed PGAWS. Moreover, using such method it is possible to estimate the phase from a total dimension of $\{(N-1)\sqrt{b}+1\} \times \{(N-1)\sqrt{b}+1\}$ by considering b bit-planes and only $N \times N$ grating dimension. Thus, this method can significantly reduce the requirement of higher spatial frequency (consequently provide more freedom to vary the parameters D_c and s) to define a grating array which would otherwise have required a high value of spatial frequency for a grating array having dimension of $\{(N-1)\sqrt{b}+1\} \times \{(N-1)\sqrt{b}+1\}$.

4. Conclusion

In conclusion, we have proposed an improved PGAWS where the duty cycle of each grating element is manipulated to control the intensity of each +1 order spot. Subsequently, we implement random binarisation of the grating array to minimise the contribution from higher order spots. Thus, the proposed PGAWS results in an array of upstanding +1 order spots where the centroid calculation accuracy increases. Through a number of simulations, we have demonstrated the working of the proposed PGAWS to generate an array of uniform intensity +1 order spots, and have also quantified the same numerically by defining a quality metric. We have further established the effectiveness of the proposed PGAWS through simulation results which demonstrate accurate wavefront estimation in comparison to the conventional PGAWS, for non-uniform intensity +1 order spots. The proposed PGAWS is expected to be useful in different fields such as biomedical imaging and laser processing, especially when the reflectivity (or transmissivity) from the sample or material under observation is non-uniform.

Acknowledgments

Author would like to acknowledge the facilities provided by University of Oxford to carry out the simulation work presented here.

ORCID iD

Biswajit Pathak https://orcid.org/0000-0001-6168-2111

References

[1] Platt B C and Shack R 2001 History and principles of Shack–Hartmann wavefront sensing *J. Refract. Surg.* **17** S573–7
[2] Liang J, Grimm B, Goelz S and Bille J F 1994 Objective measurement of wave aberrations of the human eye with the use of a Hartmann–Shack wave-front sensor *J. Opt. Soc. Am.* A **11** 1949–57
[3] Roorda A, Romero-Borja F, Donnelly III W J, Queener H, Hebert T J and Campbell M C W 2002 Adaptive optics scanning laser ophthalmoscopy *Opt. Express* **10** 405–12
[4] Wilson R W 2002 SLODAR: measuring optical turbulence altitude with a Shack–Hartmann wavefront sensor *Mon. Not. R. Astron. Soc.* **337** 103–8
[5] Cha J-W, Ballesta J and So P T C 2010 Shack–Hartmann wavefront-sensor-based adaptive optics system for multiphoton microscopy *J. Biomed. Opt.* **15** 046022
[6] Rahman S A and Booth M J 2013 Direct wavefront sensing in adaptive optical microscopy using backscattered light *Appl. Opt.* **52** 5523–32
[7] Aleksandrov A G, Zavalova V E, Kudryashov A V, Rukosuev A L, Sheldakova Y V, Samarkin V V and Romanov P N 2010 Shack–Hartmann wavefront sensor for measuring the parameters of high-power pulsed solid-state lasers *Quantum Electron.* **40** 321
[8] Müllenbroich M C, McAlinden N and Wright A J 2013 Adaptive optics in an optical trapping system for enhanced lateral trap stiffness at depth *J. Opt.* **15** 075305
[9] Southwell W H 1980 Wave-front estimation from wave-front slope measurements *JOSA* **70** 998–1006
[10] Pathak B and Boruah B R 2014 Improved wavefront reconstruction algorithm for Shack–Hartmann type wavefront sensors *J. Opt.* **16** 055403
[11] Pathak B and Boruah B R 2017 Improvement in error propagation in the Shack–Hartmann-type zonal wavefront sensors *J. Opt. Soc. Am.* A **34** 2194–202
[12] Zhao L, Bai N, Xiang Li, Ong L S, Fang Z P and Asundi A K 2006 Efficient implementation of a spatial light modulator as a diffractive optical microlens array in a digital Shack–Hartmann wavefront sensor *Appl. Opt.* **45** 90–4
[13] Bowman R W, Wright A J and Padgett M J 2010 An SLM-based Shack–Hartmann wavefront sensor for aberration correction in optical tweezers *J. Opt.* **12** 124004
[14] Podanchuk D, Dan'ko V P, Kotov M, Son J-Y and Choi Y-J 2006 Extended-range Shack–Hartmann wavefront sensor with nonlinear holographic lenslet array *Opt. Eng.* **45** 053605
[15] Boruah B R 2010 Zonal wavefront sensing using an array of gratings *Opt. Lett.* **35** 202–4
[16] Pathak B 2017 Development of a zonal wavefront sensor with enhanced performance using a reconfigurable array of binary diffraction gratings *PhD Thesis IIT Guwahati*
[17] Boruah B R and Das A 2011 Zonal wavefront sensor with reduced number of rows in the detector array *Appl. Opt.* **50** 3598–603
[18] Pathak B, Das A and Boruah B R 2012 High-speed zonal wavefront sensing *Optical Design and Testing V* vol 8557 (Int. Society for Optics and Photonics) p 85570A
[19] Pathak B and Boruah B R 2016 Zonal wavefront sensing with enhanced spatial resolution *Opt. Lett.* **41** 5600–3
[20] Pathak B and Boruah B R 2018 A zonal wavefront sensor with multiple detector planes *J. Opt.* **20** 035604
[21] Cao G and Xin Y 1994 Accuracy analysis of a Hartmann–Shack wavefront sensor operated with a faint object *Opt. Eng.* **33** 2331–6
[22] Thomas S, Fusco T, Tokovinin A, Nicolle M, Michau V and Rousset G 2006 Comparison of centroid computation algorithms in a Shack–Hartmann sensor *Mon. Not. R. Astron. Soc.* **371** 323–36
[23] Zou W and Rolland J P 2006 Quantifications of error propagation in slope-based wavefront estimations *J. Opt. Soc. Am.* A **23** 2629–38
[24] Wang S, Yang P, Bing X, Dong L and Mingwu A 2015 Shack–Hartmann wavefront sensing based on binary-aberration-mode filtering *Opt. Express* **23** 5052–64
[25] Endo T, Miwa Y, Suzuki J, Ando T, Takanezawa T and Ezaki Y 2018 Improving techniques for Shack–Hartmann wavefront sensing: dynamic-range and frame rate *The Advanced Maui Optical and Space Surveillance Conf.* pp 964–73
[26] Baranec C and Dekany R 2008 Study of a MEMS-based Shack–Hartmann wavefront sensor with adjustable pupil sampling for astronomical adaptive optics *Appl. Opt.* **47** 5155–62
[27] Xiaoyu M, Jie M, Rao C, Yang J, Rao X and Tian Y 2014 Extension of the modal wave-front reconstruction algorithm to non-uniform illumination *Opt. Express* **22** 15589–98
[28] Vohnsen B, Carmichael A, Sharmin N, Qaysi S and Valente D 2017 Volumetric integration model of the Stiles–Crawford effect of the first kind and its experimental verification *J. Vis.* **17** 18
[29] Marcos S, Diaz-Santana L, Llorente L and Dainty C 2002 Ocular aberrations with ray tracing and Shack–Hartmann wave-front sensors: does polarization play a role? *J. Opt. Soc. Am.* A **19** 1063–72
[30] Fujii T, Kougo J, Mizuno Y, Ooki H and Hamatani M 2003 Portable phase measuring interferometer using Shack–Hartmann method *Proc. SPIE* vol 5038 pp 726–32

[31] Kumar N, Khare A and Boruah B R 2020 An ex-situ surface profile measurement scheme using a zonal wavefront sensor with simultaneous presence of reference and test wavefronts *Proc. SPIE* vol 11287 p 1128719
[32] Neil M A A, Booth M J and Wilson T 1998 Dynamic wave-front generation for the characterization and testing of optical systems *Opt. Lett.* **23** 1849–51
[33] Boruah B R 2009 Dynamic manipulation of a laser beam using a liquid crystal spatial light modulator *Am. J. Phys.* **77** 331–6
[34] Mahajan V N 1994 Zernike circle polynomials and optical aberrations of systems with circular pupils *Appl. Opt.* **33** 8121–4
[35] Harvey J E and Pfisterer R N 2019 Understanding diffraction grating behavior: including conical diffraction and Rayleigh anomalies from transmission gratings *Opt. Eng., Bellingham* **58** 087105
[36] Das A and Boruah B R 2011 Point scanning microscope with adaptive illumination beam intensity *AIP Conf. Proc.* **1391** 324–6
[37] Maurer C, Schwaighofer A, Jesacher A, Bernet S and Ritsch-Marte M 2008 Suppression of undesired diffraction orders of binary phase holograms *Appl. Opt.* **47** 3994–8
[38] Benoît-Pasanau C, Goudail F, Chavel P, Cano J-P and Ballet Jôme 2010 Minimization of diffraction peaks of spatial light modulators using Voronoi diagrams *Opt. Express* **18** 15223–35
[39] Boruah B R, Love G D and Neil M A A 2011 Interferometry using binary holograms without high order diffraction effects *Opt. Lett.* **36** 2357–9
[40] Cashmore M T, Hall S R G and Love G D 2014 Traceable interferometry using binary reconfigurable holograms *Appl. Opt.* **53** 5353–8